On the Spectral Efficiency of Movable and Rotary Antenna Arrays under Rician Fading

Citation for the original published paper (version of record):
Tominaga, E., López, O., Svensson, T. et al (2025). On the Spectral Efficiency of Movable and Rotary Antenna Arrays under Rician Fading. IEEE Open Journal of the Communications Society, 6: 2642-2659. http://dx.doi.org/10.1109/OJCOMS.2025.3558304

Received 7 February 2025; revised 21 March 2025; accepted 1 April 2025. Date of publication 7 April 2025; date of current version 15 April 2025.

Digital Object Identifier 10.1109/OJCOMS.2025.3558304

On the Spectral Efficiency of Movable and Rotary Antenna Arrays Under Rician Fading

EDUARDO N. TOMINAGA [1] (Graduate Student Member, IEEE), ONEL L. A. LÓPEZ [1] (Senior Member, IEEE), TOMMY SVENSSON [2] (Senior Member, IEEE), RICHARD D. SOUZA [3] (Senior Member, IEEE), AND HIRLEY ALVES [1] (Member, IEEE)

[1] Centre for Wireless Communications, University of Oulu, 90570 Oulu, Finland
[2] Department of Electrical Engineering, Chalmers University of Technology, 412 96 Gothenburg, Sweden
[3] Department of Electrical and Electronics Engineering, Federal University of Santa Catarina, Florianópolis 88040-370, Brazil

CORRESPONDING AUTHOR: E. N. TOMINAGA (e-mail: eduardo.noborotominaga@oulu.fi)

This work was supported in part by the Research Council of Finland (former Academy of Finland), 6Genesis Flagship under Grant 346208; in part by the European Union's Horizon 2020 Research and Innovation Programme (EU-H2020), Hexa-X-II Project under Grant 101095759; in part by the Finnish Foundation for Technology Promotion, in part by the Brazil by CNPq under Grant 305021/2021-4; and in part by the RNP/MCTI Brasil 6G under Grant 01245.020548/2021-07.

ABSTRACT Most works evaluating the performance of Multi-User Multiple-Input Multiple-Output (MU-MIMO) systems consider Access Points (APs) with fixed antennas, that is, without any movement capability. Recently, the idea of APs with antenna arrays that are able to move have gained traction among the research community. Many works evaluate the communications performance of Movable Antenna Arrays (MAAs) that can move on the horizontal plane. However, they require a very bulky, complex and expensive movement system. In this work, we propose a simpler and cheaper alternative: the utilization of Rotary Antenna Arrays (RAA)s, i.e., antenna arrays that can rotate. We also analyze the performance of a system in which the array is able to both move and rotate. We focus on narrowband machine-type communications use cases in indoor scenarios, where multiple devices communicate simultaneously with the same AP in the uplink. The movements and/or rotations of the array are computed in order to maximize the mean per-user achievable spectral efficiency, based on estimates of the locations of the active devices and using particle swarm optimization. We adopt a spatially correlated Rician fading channel model, and evaluate the resulting optimized performance of the different setups in terms of mean per-user achievable spectral efficiencies. Our numerical results show that both the optimal rotations and movements of the arrays can provide substantial performance gains when the line-of-sight components of the channel vectors are strong. Moreover, the simpler RAAs can outperform the MAAs when their movement area is constrained.

INDEX TERMS MU-MIMO, Rician fading, movable antennas, rotary antennas, particle swarm optimization.

I. INTRODUCTION

MULTI-USER Multiple-Input Multiple-Output (MU-MIMO) technologies play a crucial role in contemporary wireless communication networks such as 4G LTE Advanced [1], 5G NR [2] and WiFi 6 [3]. In MU-MIMO networks, a base station or Access Point (AP) equipped with multiple antennas serve multiple active devices at the same time. By utilizing beamforming techniques, MU-MIMO provides numerous benefits, including diversity and array gains, spatial multiplexing capabilities, and interference suppression. These benefits collectively enhance the capacity, reliability, and coverage of wireless networks [4].

Most of the works[1] analyzing the performance of MU-MIMO networks consider APs equipped with Fixed Antenna Arrays (FAAs), i.e., antenna arrays with no movement

[1] Preliminary results of this work were published in the conference version [5]. In that work, we only studied rotary antenna arrays. Since the optimization problem studied in that work has only one variable (we optimize the angular position of only a single AP), brute force search was used instead of PSO.

capabilities. However, the idea of antenna arrays that can move has captured the interest of the research community [5], [6], [7], [8], [9], [10], [11], [12], [13], [14], [15], [16], [17], [18], [19], [20], [21], [22], [23], [24], [25], [26]. The goal of moving and/or rotating antennas is to take advantage of spatially varying channel conditions within a confined space. By adjusting the position and/or orientation of the antenna, better channel conditions can be achieved. In Machine-Type Communication (MTC) use cases, devices are usually deployed in fixed positions or exhibit minimal mobility, while the surrounding propagation environment changes slowly over time. Under these circumstances, narrowband MTC provides limited time and frequency diversity, constraining the potential to enhance data rates and transmission reliability. In these situations, antennas with movement capabilities offer a promising approach to achieve greater spatial diversity gains [13], [14]. In indoor scenarios, potential use cases include industrial IoT and smart homes [13]. In such use cases, a large number of devices must perform uplink transmissions to report data to the network, which can result in multiple simultaneous transmissions. Examples of such devices include surveillance cameras or smart utility meters that measure parameters like temperature, humidity, noise and carbon monoxide levels, and energy consumption of appliances.

A. RELATED WORKS

The use of antenna arrays with movement capabilities is not a completely novel concept. For example, the authors in [6] introduced a Direction of Arrival (DOA) estimation technique that employs a rotary Uniform Linear Array (ULA) of antennas. This rotary ULA performs satisfactorily for under-determined DOA estimations, where the number of source signals exceeds the number of receiving antenna elements. The performance of point-to-point Line-of-Sight (LoS) links where both the transmitter and receiver are equipped with a rotary ULA was studied in [7]. Their setup is able to approach the LoS capacity at any desired Signal-to-Noise Ratio (SNR). López et al. [8], [9] and Lin et al. [10] investigated the use of rotary ULAs for wireless energy transfer. Their study focused on a system where a power beacon (equipped with a rotary ULA) continuously rotates to transmit energy signals in the downlink to multiple devices. These devices then capture the transmitted energy to recharge their batteries. The authors in [11] designed and evaluated a prototype for hybrid mechanical-electrical beamforming in mmWave WiFi. Their experiments using a point-to-point setup demonstrated that adjusting the antenna array's orientation can substantially enhance throughput in both Line-of-Sight (LoS) and Non-Line-of-Sight (NLoS) conditions. Newly, Wu et al. [12] studied the uplink of a MU-MIMO system where the BS is equipped with a planar array of rotatable directive antennas, while the served users are equipped with fixed antennas. By jointly optimizing the 3D orientation of each antenna, their proposed methods noticeably improve the minimum SINR of the system compared to the benchmark case of BS equipped with isotropic antennas.

Recently, movable antennas, which are antennas (or antenna arrays) that can move within an one-dimensional [15], two-dimensional [18], or three-dimensional space [19], have been studied in many research works [13], [14], [15], [16], [17], [18], [19], [20], [21], [22], [27]. The authors in [15] investigated how the extra degrees-of-freedom obtained with a movable antenna array can be combined with the beamforming vector to obtain full array gain over the desired direction and null-steering over all undesired directions. Kang [16] studied a multicast scenario where a BS equipped with an linear array of movable antennas transmits a common message to multiple users, each equipped with a single fixed antenna. The antennas at the BS can move within a line segment, and their positions are optimized using deep learning techniques. Mei et al. [17] considered a MISO communication system where the transmitter is equipped with multiple movable antennas, while the receiver is equipped with a single fixed antenna. Their results showed that the optimal positions of the antennas at the transmitter significantly enhance the received SNR when compared to the case of a transmitter equipped with fixed antennas. In [18], the authors consider a point-to-point wireless communication system in which both the transmitter and the receiver are equipped with a movable antenna. Their numerical results show that the movement of the antennas can significantly increase the SNR of the wireless link in comparison with fixed antennas. In [19], the authors considered the uplink of a MU-MIMO system in which the multiple user terminals are each equipped with a single movable antenna, while the BS is equipped with an FAA. They showed that the optimal antenna positions can minimize the total transmit power of the users subject to a minimum achievable rate requirement for each user. Conversely, Wu et al. [20] studied the downlink of an MU-MIMO system where the BS is equipped with multiple movable antennas, while the each served user is equipped with a single fixed antenna. Considering discrete positions for the movable antennas, their results showed that the optimal position of the antennas can reduce the total transmit power required at the BS to ensure a minimum SINR to all the served users. Feng et al. [21] also studied the downlink of a MU-MIMO system, but considering a more complex setup where the BS is equipped with multiple movable antennas, and each served user is equipped with a single movable antenna. Their results showed that the sum rates of the system were considerable improved when compared to the cases of fixed antennas at the BS and users, fixed antennas at the BS and movable antennas at the users, and movable antennas at the BS and fixed antennas at the users. Wei et al. [22] showed that the performance of cognitive radio systems can also be improved when the secondary transmitter is equipped with an array of movable antennas. Note that the major drawback of the movable antennas studied in [13], [14], [15], [16], [17], [18], [19], [20], [21], [22].

is their difficult implementation: each movable antenna requires servo-motors, cables and slide tracks in order to move, which represents high deployment, operation and maintenance costs.

Shao et al. [25], [26] considered BSs equipped with 6D movable antenna systems for both wireless sensing and communications. Each 6D movable antenna is composed of a set of Uniform Planar Arrays (UPAs), which can be independently adjusted in terms of its 3D position and 3D rotation. They can serve both terrestrial and non-terrestrial users in outdoor settings. The results in [25] show that the 6D movable antennas significantly enhance the DoA estimation accuracy compared to isotropic or fixed directive antenna radiation patterns. Similarly, the results in [26] show that the optimal positions and rotations of the UPAs significantly improve the network capacity when compared to the benchmark case of BSs equipped with fixed arrays or with movable antennas with limited/partial movability.

Unmanned Aerial Vehicles (UAVs) functioning as flying base stations [28], [29] can also be viewed as APs equipped with movable antennas. Their key advantage lies in their high maneuverability, allowing them to be positioned at any location within the coverage area, at various heights, with easy repositioning as required. However, they face significant limitations, including restricted load capacity, substantial power consumption, and the frequent need for recharging [30].

In our previous works [5], [24], we investigated rotary ULAs in a single AP setup [5] and in different distributed MIMO setups [24]. Both works showed that, under Rician channels where the Rician factor is high, the optimal rotation of the ULAs brings substantial gains on the Spectral Efficiency (SE). However, both works did not compare the rotary antennas with other alternatives such as the movable antennas studied in [13], [14], [15], [18], [19].

In addition to rotary, movable, and flying antennas, Ning et. al. [23] discussed other possible implementations such as sliding, foldable, and even liquid antenna arrays. They emphasized that the research field of antennas with movement capabilities is still in its infancy, and that there is an urgent need to explore new and cost-effective implementations that achieves a good balance between communications performance and implementation complexity. We refer readers to [27] for a comprehensive tutorial on movable antennas, covering their historical development, channel modeling, architectures, use cases, optimization strategies, and prototyping. Note that the most noticeable advantage of rotary ULAs when compared to alternative approaches is the lower deployment, operation and maintenance costs, since they require only single servo-motor for rotation [10], [11].

B. CONTRIBUTIONS AND ORGANIZATION OF THE PAPER

The contributions of this work are summarized as follows:

- Focusing on narrowband MTC use cases in indoor scenarios, we investigate the benefits of optimally moving and/or rotating the antenna arrays in communication systems. We consider a MU-MIMO system where an AP is equipped with an array of antennas and serves multiple active devices in the uplink. We adopt a spatially correlated Rician fading channel model and the mean per-user achievable SE as the performance metric.
- We propose Rotary Antenna Arrays (RAAs) as a low cost and low complexity alternative to the Movable Antennas Arrays (MAAs) studied in the literature. While RAAs require only one servo motor for rotation, MAAs require two servo motors, cables and slide tracks to move within a plane. Both setups significantly outperform the FAA when the devices experience strong LoS conditions. Despite their simplicity, the RAA outperforms the MAA when the movement area of the latter is constrained.
- We also propose the combination of both techniques into Movable and Rotary Antenna Arrays (MRAAs),[2] which have a more complex setup but always achieve the best performance since it combines the degrees-of-freedom from both the RAA and MAA.
- We proposed a method that relies on estimates of the locations of the active devices and Particle Swarm Optimization (PSO) to compute the optimal positions and/or rotations of the antenna array. The numerical results also show that our proposed optimization method is robust against imperfect information about the location of the devices. In other words, even when the information about the location of the active devices is poor, the system still computes an optimal position and/or rotation for the antenna array that substantially increases the performance.

This paper is organized as follows. Section II presents the system and signal models, the proposed framework, the adopted performance metric and a mathematical model for the localization error. Section III presents the mechanism for optimizing the movement and/or rotation of the antenna arrays, along with the proposed location-based beamforming method employed to determine the objective function. Section IV presents and discusses the numerical results. Finally, Section V concludes the paper. Table 1 lists the acronyms used throughout this paper alphabetically.

Notation: lowercase bold face letters denote column vectors, while boldface upper case letters denote matrices. a_i is the i-th element of the column vector $\mathbf{a}$, while $\mathbf{a}_i$ is the i-th column of the matrix $\mathbf{A}$. $\mathbf{I}_M$ is the identity matrix with size $M \times M$. The superscripts $(\cdot)^T$ and $(\cdot)^H$ denote the transpose and the conjugate transpose of a vector or

[2]Our proposed MRAA shares similarities with the 6D movable antennas studied by Shao et al. [25], [26], which consist of multiple UPAs with individually adjustable 3D positions and/or rotations. In contrast, our MRAA is a simpler device designed for lower implementation and maintenance costs, equipped with a single ULA. While [25], [26] consider outdoor settings where the BS serves both terrestrial and non-terrestrial networks, we focus on an indoor scenario where the AP serves only terrestrial devices.

TABLE 1. List of acronyms.

Acronym	Definition	Acronym	Definition
AP	Access Point	NLoS	Non-LoS
CSI	Channel State Information	PSO	Particle Swarm Optimization
FAA	Fixed Antenna Array	RA	Random Access
LoS	Line-of-Sight	RAA	Rotary Antenna Array
MAA	Movable Antenna Array	SE	Spectral Efficiency
MIMO	Multiple-Input Multiple-Output	SINR	Signal-to-Interference -plus-Noise Ratio
MRAA	Movable and Rotary Antenna Array	SNR	Signal-to-Noise Ratio
MTD	Machine-Type Device	ULA	Uniform Linear Array
MU	Multi-User	ZF	Zero Forcing

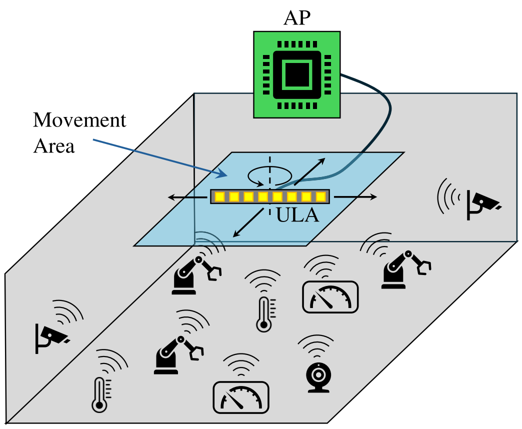

FIGURE 1. System model: an indoor industrial scenario where multiple active MTDs transmit data to an AP, which is equipped with an ULA that can move and/or rotate.

matrix, respectively. The magnitude of a scalar quantity or the cardinality of a set are denoted by $|\cdot|$. The Euclidean norm of a vector (2-norm) is denoted by $\|\cdot\|$. We denote the one dimensional uniform distribution with bounds a and b by $\mathcal{U}(a, b)$. We denote the multivariate Gaussian distribution with mean $\mathbf{a}$ and covariance $\mathbf{B}$ by $\mathcal{N}(\mathbf{a}, \mathbf{B})$.

II. SYSTEM MODEL

We consider an indoor[3] square coverage area with dimensions $L_A \times L_A$ m^2. The coverage area is served by a single Access Point (AP) equipped with a Uniform Linear Array (ULA) of M half-wavelength spaced antenna elements, and placed at height h_{AP}. The AP is located at the center of the coverage area, i.e., $\mathbf{p}_{\text{AP}} = (L_A/2, L_A/2)$.

[3]In an indoor scenario, the MAA can move on the ceiling of the coverage area. In an alternative outdoor scenario, the MAA would be able to move on the top or on the façade of a building.

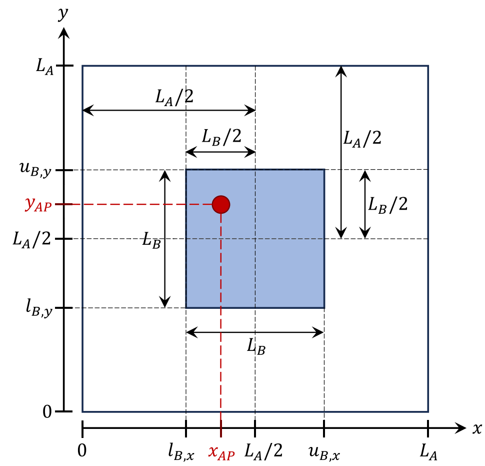

FIGURE 2. Illustration of the movement area of the MAAs (blue square). The red dot represents the position of the MAA.

The AP serves K active Machine-Type Devices (MTDs) simultaneously. Let $\mathbf{p}_k = (x_k, y_k)^T$ denote the coordinates of the k-th MTD, assuming for simplicity that all devices are located at the same height h_{device} [31], [32].

The AP can be equipped with one of four different types of antenna arrays:

1) *FAA:* the antenna array has no movement capabilities.
2) *RAA:* the antenna array is able to rotate.
3) *MAA:* the antenna array is able to move on the horizontal plane.
4) *MRAA:* the antenna array can both rotate and move on the horizontal plane.

The system model is illustrated in Fig. 1. The MAAs and MRAAs are able to move within a square area with dimensions $L_B \times L_B$ that is inscribed on the square coverage area, as illustrated in Fig. 2. Finally, Fig. 3 shows illustrations of the MAA and MRAA systems. Note that the RAA is equipped with a single servo motor, while the MAA has two servo motors, cables, and slide tracks. The MRAA has the same movement apparatus of the MAA, but equipped with an additional third servo motor that rotates the array.

A. CHANNEL MODEL

All the antenna mechanisms studied in this work (FAA, RAA, MAA, and MRAA) utilize an ULA with M antenna elements. They differ on the capabilities to move and/or rotate the ULA. Besides, the position and/or orientation of the ULA are kept constant during multiple coherence time intervals. Then, the adopted channel model describes the vector of wireless channel coefficients (within a single coherence interval) between an active MTD at a given location (x_k, y_k) and an ULA with a given orientation and whose mid-point is at a given position $(x_{\text{AA}}, y_{\text{AA}})$. Consequently, the distance d_k between the ULA and the MTD and the angle ϕ_k between the boresight of the ULA and the MTD depend on those given parameters.

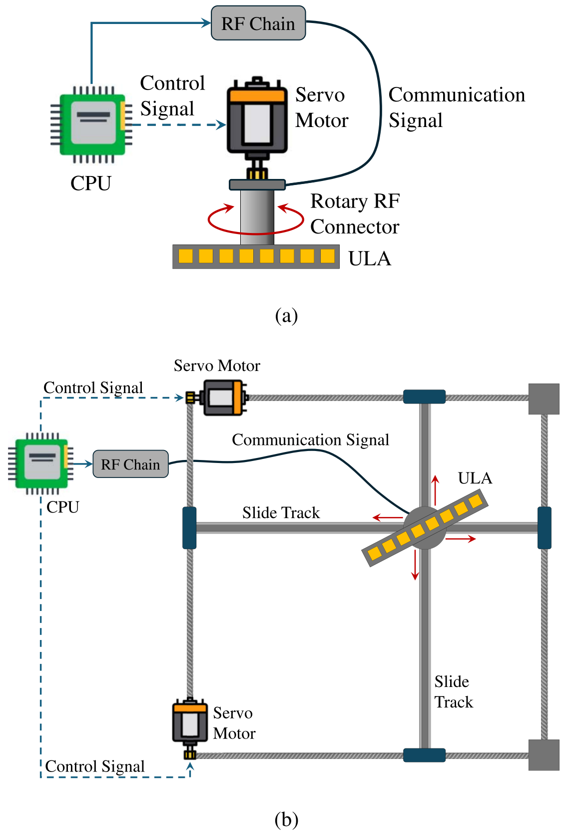

FIGURE 3. Illustration of (a) RAA and (b) MRAA systems [13]. The antenna array is an ULA of $M = 8$ antenna elements.

We adopt a spatially correlated Rician fading channel model [33]. Let $\mathbf{h}_k \in \mathbb{C}^{M\times 1}$ denote the channel vector between the k-th MTD and the AP. It can be modeled as [34]

$$\mathbf{h}_k = \sqrt{\frac{\kappa}{1+\kappa}}\mathbf{h}_k^{\text{los}} + \sqrt{\frac{1}{1+\kappa}}\mathbf{h}_k^{\text{nlos}}, \tag{1}$$

where κ is the Rician factor, $\mathbf{h}_k^{\text{los}} \in \mathbb{C}^{M\times 1}$ is the deterministic LoS component, and $\mathbf{h}_k^{\text{nlos}} \in \mathbb{C}^{M\times 1}$ is the random NLoS component. Note that term $\mathbf{h}_k^{\text{NLoS}}$ in (1) comprises the multi-path components of the channel vector. The Rician factor κ determines the power ratio between the LoS component and the sum of the multi-path components.

The deterministic LoS component is given by

$$\mathbf{h}_k^{\text{los}} = \sqrt{\beta_k}\begin{bmatrix} 1 \\ \exp(-j2\pi\Delta\sin(\phi_k)) \\ \exp(-j4\pi\Delta\sin(\phi_k)) \\ \vdots \\ \exp(-j2\pi(M-1)\Delta\sin(\phi_k)) \end{bmatrix}, \tag{2}$$

where β_k is the power attenuation due to the distance between the k-th MTD and the AP, Δ is the normalized inter-antenna spacing, and $\phi_k \in [0, 2\pi]$ is the azimuth angle relative to the boresight of the ULA of the AP. Meanwhile, the random NLoS component is distributed as

$$\mathbf{h}_k^{\text{nlos}} \sim \mathcal{CN}(\mathbf{0}, \mathbf{R}_k). \tag{3}$$

Note that

$$\mathbf{h}_k \sim \mathcal{CN}\left(\sqrt{\frac{\kappa}{1+\kappa}}\mathbf{h}_k^{\text{los}}, \frac{\mathbf{R}_k}{\kappa+1}\right), \tag{4}$$

where $\mathbf{R}_k \in \mathbb{C}^{M\times M}$ with $\text{Tr}(\mathbf{R}_k) = \beta_k$ is the positive semi-definite covariance matrix describing the spatial correlation of the NLoS components.

The spatial covariance matrices can be (approximately) modeled using the Gaussian local scattering model [35, Sec. 2.6]. Specifically, the s-th row, m-th column element of the correlation matrix is

$$[\mathbf{R}_k]_{s,m} = \frac{\beta_k}{N}\sum_{n=1}^{N}\exp\left[j\pi(s-m)\sin(\psi_{k,n})\right] \times \exp\left\{-\frac{\sigma_\phi^2}{2}[\pi(s-m)\cos(\psi_{k,n})]^2\right\}, \tag{5}$$

where N is the number of scattering clusters, $\psi_{k,n}$ is the nominal Angle of Arrival (AoA) for the n-th cluster, and σ_ψ is the Angular Standard Deviation (ASD).

To take advantage of its multiple antennas, the AP must estimate the channel responses of the active MTDs. Channel estimation is often performed using pilot sequences that the UEs transmit in the uplink and are known to the AP [35]. In practice, the channel estimates are not perfect, i.e., there is a channel estimation error associated to them. The estimated channel vector of the k-th MTD, $\hat{\mathbf{h}}_k \in \mathbb{C}^{M\times 1}$, can be modeled as the sum of the true channel vector plus a random error vector as [36], [37], [38]

$$\hat{\mathbf{h}}_k = \mathbf{h}_k + \tilde{\mathbf{h}}_k, \tag{6}$$

where $\tilde{\mathbf{h}}_k \sim \mathcal{CN}(\mathbf{0}, \sigma_{\text{csi}}^2\mathbf{I})$ is the vector of channel estimation errors. Note that the true channel realizations and the channel estimation errors are uncorrelated.

The parameter σ_{csi}^2 indicates the quality of the channel estimates. Let

$$\rho = \frac{p}{\sigma_n^2} \tag{7}$$

denote the per-antenna transmit SNR, where $p \geq 0$ is the fixed uplink transmit power (which is the same for all the devices) and σ_n^2 is the receive noise power at the APs. We assume that there are τ_p orthogonal pilot sequences during the uplink data transmission phase, such that $\tau_p \geq K$. We also assume that the duration of the uplink pilot transmission phase is equal to τ_p symbols. Then, variance of the channel estimation errors can be modeled as a decreasing function of ρ as [36], [37], [38]

$$\sigma_{\text{csi}}^2 = \frac{1}{\tau_p\rho}. \tag{8}$$

Note that the channel estimation error depends only on the uplink transmit power, receive noise power and number of orthogonal pilots, thus it is the same for all devices.

B. PROPOSED FRAMEWORK

In this subsection, we describe our proposed framework for the optimization of the rotation and/or position of the antenna array and uplink data transmission. Similarly to the frameworks adopted in [39] and [24], our framework has the following phases:

1) Active MTDs, that is, those attempting to transmit data to the network, transmit non-orthogonal uplink pilots for activity detection.
2) The AP detects the set of active MTDs and uses indoor localization techniques to estimate their locations.
3) Assuming pure LoS propagation, the AP uses the estimated locations of the MTDs along with location-based beamforming to calculate its optimal rotation and/or position. After the calculation, the antenna array is moved and/or rotated.
4) The AP broadcasts a common downlink feedback message to assign each MTD an orthogonal pilot sequence.
5) The MTDs transmit their orthogonal pilot sequences along with data during multiple consecutive time slots. The uplink orthogonal pilots are used to compute the CSI estimates shown in (6) for each coherence time interval, which are then used to compute the ZF receive combining vectors in (14).

The proposed framework is depicted in Fig. 4. Phase 5 spans T time slots, where K active devices transmit simultaneously during each time slot. Moreover, the length of each time slot is equal to the channel's coherence time interval and consists of τ_c symbols. The first τ_p symbols of each time slot are allocated for the transmission of orthogonal pilot sequences, while the remaining $\tau_d = \tau_c - \tau_p$ symbols are used for uplink data transmission. The numerical results presented in this work, specifically the mean per-user achievable SE in Section II-D, reflect the uplink communication performance during phase 5.

C. SIGNAL MODEL

The matrix $\mathbf{H} \in \mathbb{C}^{M\times K}$ containing the channel vectors of the K devices transmitting their data to the AP can be written as

$$\mathbf{H} = [\mathbf{h}_1, \mathbf{h}_2, \dots, \mathbf{h}_K]. \tag{9}$$

Then, the $M \times 1$ received signal vector can be written as

$$\mathbf{y} = \sqrt{p}\mathbf{H}\mathbf{x} + \mathbf{n}, \tag{10}$$

where $\mathbf{x} \in \mathbb{C}^{K\times 1}$ is the vector of symbols simultaneously transmitted by the K devices, and $\mathbf{n} \in \mathbb{C}^{M\times 1}$ is the vector of additive white Gaussian noise samples such that $\mathbf{n} \sim \mathcal{CN}(\mathbf{0}_{M\times 1}, \sigma_n^2\mathbf{I}_M)$.

Let $\mathbf{V} \in \mathbb{C}^{M\times K}$ be a linear detector matrix used for the joint decoding of the signals transmitted from the K devices. The received signal after the linear detection operation is split to K streams and given by

$$\mathbf{r} = \mathbf{V}^H\mathbf{y} = \sqrt{p}\mathbf{V}^H\mathbf{H}\mathbf{x} + V^H\mathbf{n}. \tag{11}$$

Let r_k and x_k denote the k-th elements of $\mathbf{r}$ and $\mathbf{x}$, respectively. Then, the received signal corresponding to the k-th MTD can be written as

$$r_k = \underbrace{\sqrt{p}\mathbf{v}_k^H\mathbf{h}_k x_k}_{\text{Desired signal}} + \underbrace{\sqrt{p}\mathbf{v}_k^H\sum_{k'\neq k}^{K}\mathbf{h}_{k'}x_{k'}}_{\text{Inter-user interference}} + \underbrace{\mathbf{v}_k^H\mathbf{n}}_{\text{Noise}}, \tag{12}$$

where $\mathbf{v}_k$ and $\mathbf{h}_k$ are the k-th columns of the matrices $\mathbf{V}$ and $\mathbf{H}$, respectively. From (12), the signal-to-interference-plus-noise ratio of the uplink transmission from the k-th MTD is given by

$$\gamma_k = \frac{p|\mathbf{v}_k^H\mathbf{h}_k|^2}{p\sum_{k'\neq k}^{K}|\mathbf{v}_k^H\mathbf{h}_{k'}|^2 + \sigma_n^2\|\mathbf{v}_k^H\|^2}. \tag{13}$$

The receive combining matrix $\mathbf{V}$ is computed as a function of the matrix of estimated channel vectors $\hat{\mathbf{H}} \in \mathbb{C}^{M\times K}$, $\hat{\mathbf{H}} = [\hat{\mathbf{h}}_1, \dots, \hat{\mathbf{h}}_K]$. In this work, we adopt Zero Forcing (ZF) combining.[4] The receive combining matrix is computed as [41]

$$\mathbf{V} = \hat{\mathbf{H}}(\hat{\mathbf{H}}^H\hat{\mathbf{H}})^{-1}. \tag{14}$$

Note that the distances and angles between the K active MTDs and the ULA change according to the adopted position and/or rotation of the ULA. Nevertheless, during the data transmission phase, the ULA is kept static. The system relies on digital beamforming for data transmission: there is one RF chain connected to each of the M antennas at the ULA, thus up to M active MTDs can be served simultaneously. At the beginning of each coherence time interval, the AP obtains the CSI from the K served MTDs using orthogonal uplink pilots. Then, the AP adopts ZF processing and compute K different receive combining vectors, that is, one receive beamforming vector for each MTD. Thanks to the ZF processing, when decoding the signal transmitted by any active MTD, a radiation pattern with a main lobe on the direction of the MTD of interest and nulls on the direction of the interfering MTDs is virtually created. This processing is performed for all the K active MTDs on each coherence time interval during the data transmission phase.

D. PERFORMANCE METRICS

We adopt as the performance metric the per-user mean achievable uplink Spectral Efficiency (SE). The achievable uplink SE of the k-th MTD is [41]

$$R_k = \frac{\tau_d}{\tau_c}\mathbb{E}_{\mathbf{H}}\{\log_2(1+\gamma_k)\}. \tag{15}$$

The expectation is taken with respect to several realizations of the channel matrices $\mathbf{H}$, which includes the effects of both LoS and NLoS propagation.

[4]MMSE combining is the optimal linear receive combining scheme. However, its implementation requires statistical knowledge of the noise and interference [35]. Besides, the performance difference between ZF and MMSE is negligible in the high SNR regime [40].

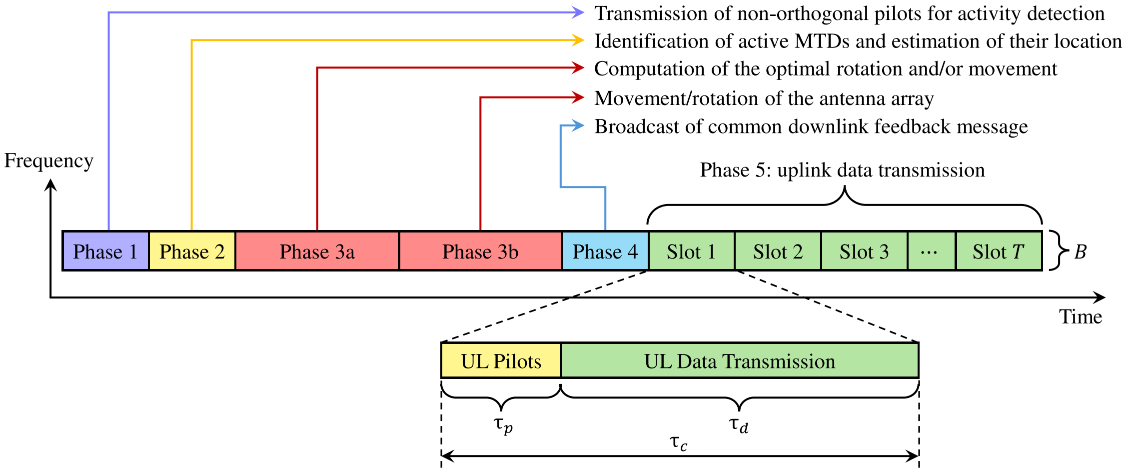

FIGURE 4. Illustration of the proposed framework for optimization of the rotation and/or position of the antenna array and uplink data transmission.

Then, the per-user mean achievable uplink SE is obtained by averaging over the achievable uplink SE of the K devices, i.e.,

$$\bar{R} = \frac{1}{K}\sum_{k=1}^{K} R_k. \tag{16}$$

In this work, we assume that the MTDs are, for instance, smart utility meters or surveillance cameras, and that the same set of MTDs transmit data to the AP simultaneously over a period of time that can span several time slots. Thus, we assume that the time spent during phases 1-4 is negligible compared to the duration of the data transmission phase, thus we consider the achievable SE only during the phase 5 as the performance metric. Nevertheless, both the surrounding environment and the set of active MTDs transmitting data may change over time, making it essential for the AP to have an antenna array with movement and/or rotation capabilities to adapt to such dynamic conditions and enhance the data rates for all MTDs.

E. LOCALIZATION ERROR MODEL

The localization error model aims at modeling the imperfect information about the location of the active devices, which is an impairment that would be encountered in practical networks. We adopt the same model that was utilized in our previous works [5], [24]. Considering that all the devices are at the same height h_{device}, imperfect localization refers to the uncertainty on the location of the devices only on the (x, y) directions. Let $\hat{\mathbf{p}}_k = (\hat{x}_k, \hat{y}_k)$ denote the estimated location of the k-th MTD. The localization error vector associated to the k-th MTD can be modeled as

$$\mathbf{e}_k = \mathbf{p}_k - \hat{\mathbf{p}}_k = (x_{e,k}, y_{e,k}), \tag{17}$$

where

$$x_{e,k} = x_k - \hat{x}_k, \tag{18}$$
$$y_{e,k} = y_k - \hat{y}_k \tag{19}$$

are the x and y components of the localization error vector, respectively.

To ensure generality and avoid introducing any additional assumptions or biases related to indoor localization in our system model, we model the localization error as a bivariate Gaussian distribution. This choice is made because the bivariate Gaussian is the least informative distribution for a given variance [42]. The localization error has mean $\boldsymbol{\mu} = [\mathbf{0}\ \mathbf{0}]^T$ and covariance matrix $\boldsymbol{\Sigma} = \sigma_e^2\mathbf{I}_2$ [43]. Then, the x and y components of the localization error vector follow a Normal distribution:

$$x_{e,k}, y_{e,k} \sim \mathcal{N}(0, \sigma_e^2). \tag{20}$$

Note that the localization error model does not impact the optimization of the position and/or rotation of the antenna array. The estimated locations of the active devices are used to compute the optimal position and/or rotation of the antenna array. As a result, the computed optimal position and/or rotation slightly deviate from those that would be obtained if the system had the perfect information about the location of the active devices. Moreover, the localization error does not affect the mean per-user achievable SE directly. In the case of FAAs, the imperfect information about the locations of the active MTDs has no effect. In the case of RAAs, MAAs, and MRAAs, rotating and/or moving the array to a sub-optimal orientation/position diminishes the potential gains on the SE obtained via the spatially varying channel conditions.

F. LOCALIZATION ACCURACY REQUIREMENTS

Let $r_{e,k} = \|\mathbf{e}_k\|$, i.e., the length of the localization error vector, represent a measure of the inaccuracy of the localization. Considering the bivariate Gaussian model, the length of the localization error vector follows the Rayleigh distribution, that is,

$$f_R(r|\sigma_e^2) = \frac{r}{\sigma_e^2}\exp\left(-\frac{r^2}{2\sigma_e^2}\right),\ r \geq 0, \tag{21}$$

where σ_e^2 is the scaling parameter. Consequently, we have

$$\mathbb{E}\{r_{e,k}\} = \sigma_e\sqrt{\pi/2}, \tag{22}$$

$$\mathrm{Var}\{r_{e,k}\} = \frac{4-\pi}{2}\sigma_e^2. \tag{23}$$

In 3GPP standards, the localization accuracy requirements are typically specified in terms of the 95%-quantile [44]. The F-quantile of a Rayleigh distribution with scaling parameter σ_e is given by

$$Q(F;\sigma_e) = \sigma_e\sqrt{-2\ln(1-F)}. \tag{24}$$

In 3GPP Rel-16, the localization accuracy requirement specified for indoor scenarios is 3 m [45], which corresponds to $\sigma_e^2 = 1.76$ dB in our localization error model. In 3GPP Rel-17, this requirement was further reduced to 20 cm [46], corresponding to $\sigma_e^2 = -21.75$ dB.

In indoor scenarios, current 4G and 5G systems present localization accuracy on the order of 10 m and 1 m, respectively [47]. Such accuracies correspond to $\sigma_e^2 = 12.22$ dB in 4G and $\sigma_e^2 = -7.77$ dB in 5G. The localization accuracy for beyond-5G and 6G networks in indoor scenarios is expected to be in the order of 1 cm [47], [48], which corresponds to $\sigma_e^2 < -40$ dB. The combination of different measurements and techniques for localization allows such levels of accuracy to be feasible [48].

III. OPTIMIZATION OF THE POSITION AND ROTATION

In each time slot, K distinct devices are active. For each subset of K locations of active devices, there is a distinct optimal rotation and/or optimal position for the antenna array.

Let $(x_{\mathrm{AA}}^0, y_{\mathrm{AA}}^0)$ denote the initial position of the array, and let $\theta_{\mathrm{AA}} \in [0,\pi]$ denote its rotation. The initial angle between the k-th active MTD and the boresight of the ULA (that is, before movement and/or rotation of the array) is

$$\phi_k = \tan^{-1}\left(\frac{y_k - y_{\mathrm{AA}}^0}{x_k - x_{\mathrm{AA}}^0}\right). \tag{25}$$

The position of the array after its movement can be written as

$$x'_{\mathrm{AA}} \coloneqq x_{\mathrm{AA}}^0 + \Delta x_{\mathrm{AA}}, \tag{26}$$

$$y'_{\mathrm{AA}} \coloneqq y_{\mathrm{AA}}^0 + \Delta y_{\mathrm{AA}}. \tag{27}$$

Besides, the final angle between the array the k-th active MTD after the movement and rotation is

$$\phi'_k = \tan^{-1}\left(\frac{y_k - y'_{\mathrm{AA}}}{x_k - x'_{\mathrm{AA}}}\right) + \theta_{\mathrm{AA}}. \tag{28}$$

In the case of a RAA, the initial and final positions of the array is the same, thus the final angle can be rewritten as

$$\phi'_k \coloneqq \phi_k + \theta_{\mathrm{AA}}. \tag{29}$$

The array and its position with respect to an active MTD, before and after its movement and rotation, is illustrated in Fig. 5.

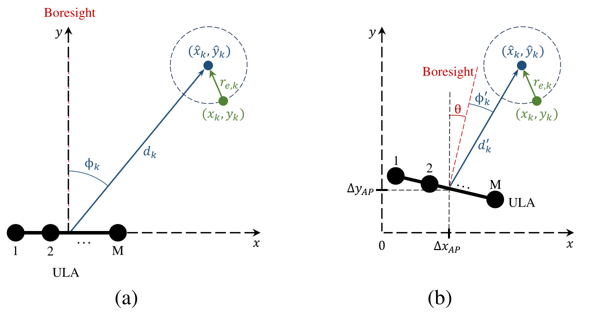

FIGURE 5. Illustration of the ULA of an AP and its position and rotation with respect to one active MTD (a) before movements (b) after movements. The green circle represents the true location of the device, and the blue circle represents the estimated location.

The variables $(x'_{\mathrm{AA}}, y'_{\mathrm{AA}}, \theta_{\mathrm{AA}})$ can be jointly optimized. The optimization problem can be written as

$$\begin{aligned} &\text{maximize} \ f(x'_{\mathrm{AA}}, y'_{\mathrm{AA}}, \theta_{\mathrm{AA}} \mid \hat{\mathbf{p}}_k, \forall k) \\ &\text{subject to} \ l_B \le x_{\mathrm{AA}}, y_{\mathrm{AA}} \le u_B, \\ &\qquad\qquad 0 \le \theta_{\mathrm{AA}} \le \pi, \end{aligned} \tag{30}$$

where $f(\cdot)$ is the objective function to be maximized, and l_B and u_B are, the lower and upper bounds, respectively, for the movements of the array in both x and y directions. The mechanism utilized to obtain the objective function is described in Section III-A. Given the estimates of the locations of the active MTDs, $\hat{\mathbf{p}}_k \ \forall k \in \{1,\ldots,K\}$, we aim at obtaining the position and/or rotation of the array (that is, the variables x_{AP}, y_{AP}, and θ_{AA}) that maximizes $f(\cdot)$. Considering that the MAA and the MRAA can move only within a square[5] with dimensions $L_B \times L_B$, inscribed on the square coverage area with dimensions $L_A \times L_A$, the lower and upper bounds for both $x_{\mathrm{AA}}, y_{\mathrm{AA}}$ are respectively given by

$$l_B = \frac{L_A - L_B}{2}, \tag{31}$$

$$u_B = \frac{L_A + L_B}{2}. \tag{32}$$

Considering the symmetry of radiation pattern of the ULA, the rotation of the array is bounded in the range $\theta_{\mathrm{AA}} \in [0,\pi]$ rad.

A. LOCATION-BASED BEAMFORMING

In this subsection, we present the mechanism utilized to compute the objective function $f(\cdot)$, which is maximized using PSO. Given the estimates of the locations of all active MTDs, that is, $\hat{\mathbf{p}}_k$, $\forall k$, we adopt a location-based beamforming [49], [50], [51], [52] approach to determine $f(\cdot)$ as a function of the position and rotation of the antenna array.

We assume that the same set of active devices transmits data over multiple consecutive coherence time intervals. In

[5] Note that the square movement area with dimensions $L_B \times L_B$ refers to all the possible points where the mid-point of the ULA can be positioned. If the mid-point of the ULA is close to one of the corners of the square movement area, parts of the ULA may be projected outside the area.

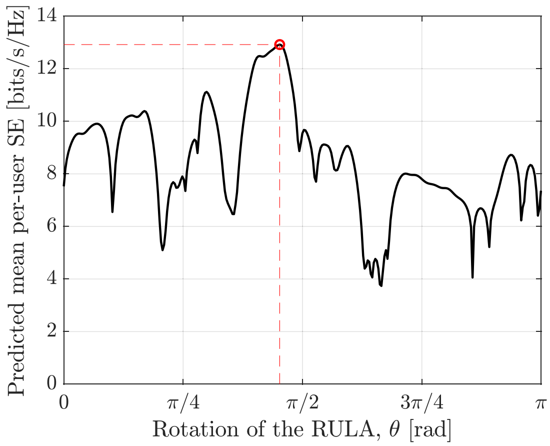

FIGURE 6. Objective function of the RAA, for $L_A = 100$ m, $M = 16$, and $K = 10$.

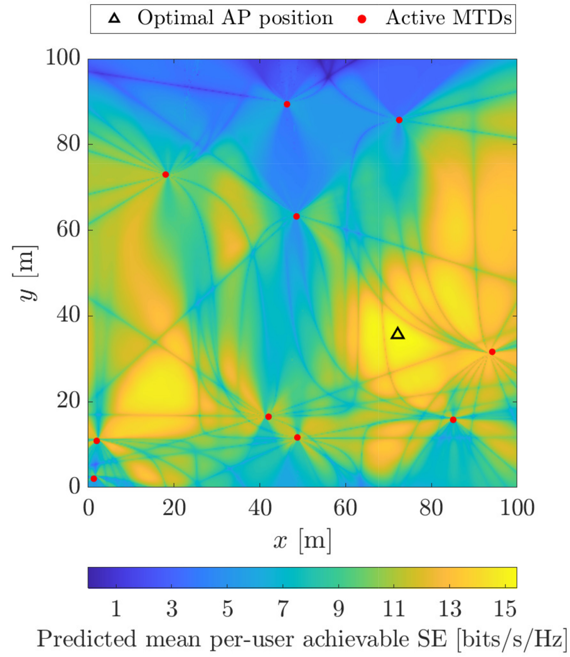

FIGURE 7. Objective function of the MAA, for $L_A = L_B = 100$ m, $M = 16$, and $K = 10$.

this case, the optimization is performed solely based on the predicted LoS component of the channel vectors because it is deterministic, that is, it is constant over several coherence time intervals. Shadowing occurs when the LoS component of the signal is blocked or attenuated by obstacles. The coherence time of the shadowing depends on the mobility of the devices and potential obstructions in the indoor scenario, such as people, vehicles, robots or machines. For the performance evaluations conducted in this work, we assume that the devices and surrounding environment are both static. In the case of low mobility, the coherence time of the shadowing is expected to be on the order of seconds. Such coherence time would still be sufficient for the entire optimization process and multiple uplink transmissions to occur. If we perform the optimization of the rotation and/or position of the APs based on the instantaneous CSI, we would need to do it on every coherence time interval, which would be impractical considering the mechanical limitations of the proposed movable and rotary systems.

Based on $\hat{\mathbf{p}}_k$, $\forall k$, the AP computes the estimates for the distances and azimuth angles between the antenna array and the MTDs, i.e., $\hat{d}_k$ and $\hat{\phi}_k$, $\forall k$. Then, it computes pseudo channel vectors assuming pure LoS propagation as

$$\mathbf{h}_k^{\text{pseudo}} = \sqrt{\hat{\beta}_k} \begin{bmatrix} 1 \\ \exp(-j2\pi\Delta\sin(\hat{\phi}_k)) \\ \exp(-j4\pi\Delta\sin(\hat{\phi}_k)) \\ \vdots \\ \exp(-j2\pi(S-1)\Delta\sin(\hat{\phi}_k)) \end{bmatrix}. \quad (33)$$

Note that the estimated large-scale fading coefficient $\hat{\beta}_k$ is computed as a function of the estimated distances $\hat{d}_k$ assuming a known channel model. Receive combining vectors are then computed as a function of the pseudo channel vectors according to (14). Finally, the objective function is obtained by computing the predicted mean-per user achievable SE utilizing the pseudo-channel vectors from (33) and the corresponding receive combining vectors in (13), (15), and (16). The objective function corresponds to the predicted mean per-user achievable SE, which is predicted assuming full LoS propagation, versus the rotation and/movement of the array.[6]

Considering a single network realization, i.e., a single set of locations of K active MTDS, we numerically evaluate the objective functions to be optimized. In Fig. 6, we show the objective function for the case of a RAA, which is the predicted mean per-user achievable SE versus the rotation of the AP. Moreover, Fig. 7 shows the objective function for the case of a MAA, which is the predicted mean per-user achievable SE for all the points of the square coverage area. Finally, Fig. 8 shows the optimal positions and/or rotations of the different setups for different network realizations, i.e., sets of locations of active MTDs, considering $L_A = L_B = 100$ m and $K = 10$.

Note that both objective functions in Figs. 6 and 7 present several local minimum and maximum points. Thus, it is not possible to obtain the optimal points utilizing, for instance, convex optimization techniques [53]. For this reason, in order to obtain the optimal rotation and/or position of the array, we employ PSO,[7] which will be presented in the next subsection.

B. PARTICLE SWARM OPTIMIZATION

PSO [54, Ch. 16] is an optimization algorithm highly effective for tackling highly non-linear optimization problems.

[6]Note that this location-based beamforming approach, which relies on the pseudo-channel vectors from (33), is utilized only to compute the optimal rotation and/or position of the antenna array. The final performance metrics consider channel estimates that are obtained with pilot sequences transmitted in the uplink. The real mean per-user achievable SE is then computed using the estimated channel vectors in (13) and (14).

[7]The obtained solution is not proven to be optimal, but PSO has been used in numerous non-convex optimization problems showing near optimal performance.

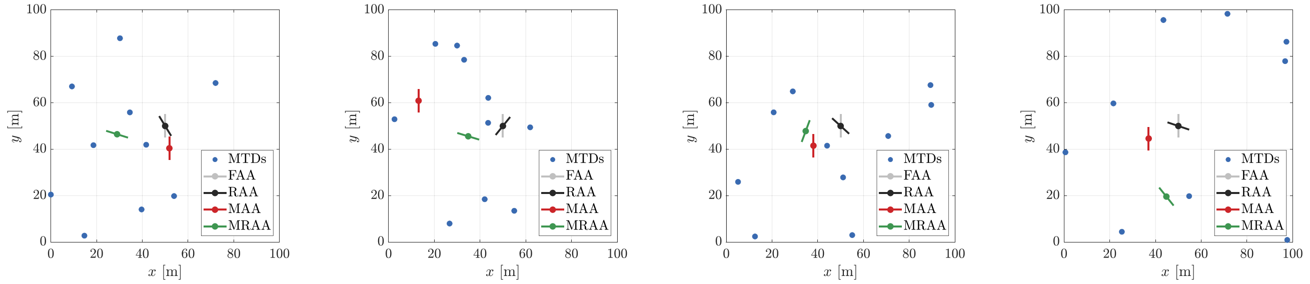

FIGURE 8. The optimal positions and/or rotations of the different setups for different network realizations, considering $L_A = L_B = 100$ m and $K = 10$.

TABLE 2. Parameters of the PSO algorithm.

Symbol	Parameter	Symbol	Parameter
$f(\cdot)$	Objective function	c_2	Social constant
x_i	Position of the i-th particle	$p_{b,i}$	Personal best of the i-th particle
v_i	Velocity of the i-th particle	g_b	Global best
w	Inertial weight	r_1, r_2	Random numbers between 0 and 1
c_1	Cognitive constant		

The algorithm begins by creating a population of candidate solutions, referred to as agents or particles, randomly distributed over the domain of the objective function. The dimension of the domain is equal to the number of variables being jointly optimized. Each particle is also initialized with a random velocity, which determines the direction and distance to the next position of the particle. At each iteration, the objective function is evaluated at each particle's position, and the algorithm determines the own best-known position for each particle and also the global best-known position among all particles. Then, the algorithm computes new velocities for each particle based on their individual best positions and also the global best position. Finally, the particles move to their next positions at the end of the iteration. After multiple iterations, the swarm of particles moves towards the optimal solution to the problem, which is the global maximum or minimum of the objective function. The iterations proceed until the algorithm reaches a stopping criterion, which can be: i) the maximum number of iterations is reached, or ii) the relative change in the value of the global best over a predefined number of stall iterations is less than a tolerance value. By exploring the diversity of positions and velocities in the swarm with properly adjusted parameters, PSO avoids converging prematurely to a local best position instead of the global best position.

The PSO was first introduced in [55], designed to simulate social behaviors such as the motion in bird flocks or fish schools. It has been applied to a variety of optimization problems in communication systems, such as optimal deployment, node localization, clustering, and data aggregation in wireless sensor networks [56]. Additionally, it has been utilized in antenna design to achieve a specific side-lobe level or to determine the positions of antenna elements in a non-uniform array [57]. It has also proven useful in computing the optimal precoding vector to maximize the throughput of a MU-MIMO system [58], optimizing scheduling in the downlink of MU-MIMO systems [59], and initializing channel estimates for MIMO-OFDM receivers that simultaneously perform channel estimation and decoding [60].

The parameters of the PSO algorithm are listed in Table 2. Moreover, a pseudo-code[8] for the PSO algorithm is listed in Algorithm 1. The inertial weight w controls the particle's tendency to continue in its current direction. Parameters c_1 and c_2 are the acceleration coefficients, and controls the influence of the personal and global best positions, respectively. The termination criterion might be a pre-determined maximum number of iterations, a certain threshold of the objective function $f(\cdot)$, or any other criteria related to the optimization problem.

The complexity of PSO is determined by the number of particles, the dimensions of the problem (that is, number of optimization variables) and the number of iterations required to achieve convergence. Thus, the complexity of PSO per iteration is $\mathcal{O}(|\mathcal{A}|N_{\text{vars}})$, where $|\mathcal{A}|$ is the swarm size (number of particles) and N_{vars} is the number of optimization variables [60]. Note that there exists a trade-off between the swarm size and the number of iterations required to achieve convergence. In the case of using only one particle, the computationally complexity per iteration is minimized but the number of iterations is maximized. On the other hand, utilizing an infinite number of particles minimizes the number of iterations but maximizes the complexity per iteration (this case would be equivalent to an exhaustive search) [60].

C. PSO VERSUS BRUTE FORCE SEARCH

In this subsection, we compare the average computational time required in MATLAB to determine the optimal position and/or rotation of the antenna array using Brute Force (BF) search and PSO. Let δ_θ denote the resolution of the antenna

[8] In this work, the PSO algorithm was implemented using the function `particleswarm` from MATLAB [61]. According to the documentation of this function [62], it guarantees that the solution of the problem is feasible by enforcing the bounds right after updating the positions of the particles.

Algorithm 1 Particle Swarm Optimization for x, y, and θ

Initialize swarm:
for each particle i in the swarm **do**
  Initialize position $\mathbf{p}_i = (x_i, y_i, \theta_i)$ randomly
  Initialize velocity $\mathbf{v}_i = (v_{x_i}, v_{y_i}, v_{\theta_i})$ randomly
  Initialize personal best position $\mathbf{p}_{b,i} = (x_{b,i}, y_{b,i}, \theta_{b,i})$ to the initial position
end for
Initialize global best position $\mathbf{g}_b = (x_{gb}, y_{gb}, \theta_{gb})$ to the best initial particle position
while Stopping criterion is not met **do**
  for each particle i in the swarm **do**
    for each dimension (x, y, θ) **do**
      Update velocity:
      $v_{x_i} = wv_{x_i} + c_1 r_1 (x_{b,i} - x_i) + c_2 r_2 (x_{gb} - x_i)$
      $v_{y_i} = wv_{y_i} + c_1 r_1 (y_{b,i} - y_i) + c_2 r_2 (y_{gb} - y_i)$
      $v_{\theta_i} = wv_{\theta_i} + c_1 r_1 (\theta_{b,i} - \theta_i) + c_2 r_2 (\theta_{gb} - \theta_i)$
    end for
    Update position:
    $x_i = x_i + v_{x_i}$
    $y_i = y_i + v_{y_i}$
    $\theta_i = \theta_i + v_{\theta_i}$
    if x_i, y_i or θ_i is outside the bounds **then**
      Set x_i, y_i or θ_i equal to the closest bound
      if The velocity of x_i, y_i or θ_i points outside the bound **then**
        Set the velocity of the component to zero
      end if
    end if
    if $f(\mathbf{p}_i)$ is better than $f(\mathbf{p}_{b,i})$ **then**
      Update personal best: $\mathbf{p}_{b,i} = (x_i, y_i, \theta_i)$
      if $f(\mathbf{p}_{b,i})$ is better than $f(\mathbf{g}_b)$ **then**
        Update global best: $\mathbf{g}_b = (x_{b,i}, y_{b,i}, \theta_{b,i})$
      end if
    end if
  end for
end while
return global best position $\mathbf{g}_b = (x_{gb}, y_{gb}, \theta_{gb})$

array's rotation, and $\delta_{x,y}$ denote the resolution of its linear movement in the x and y directions. The results obtained for the RAA, MAA, and MRAA with different resolution settings are presented in Tables 3, 4, and 5, respectively. Considering practical implementations, we assume a small movement area with $L_B = 1$ m for the MAA/MRAA cases.

In the case of the RAA, determining the optimal angular position of the array requires solving a one-dimensional optimization problem. Consequently, BF search may be faster than PSO unless the quantization level is very high, as shown in Table 3. For the MAA, computing the optimal position requires solving a two-variable joint optimization problem, while for the MRAA, determining the optimal position and rotation involves solving a three-variable joint optimization problem. As shown in Tables 4 and 5, PSO

TABLE 3. Average time required to compute the optimal rotation of the RAA using different optimization strategies, for $l = 100$ m and $K = 10$.

Optimization strategy	Average computational time
PSO	0.1025 s
BF, $\delta_\theta = 1°$	0.0133 s
BF, $\delta_\theta = 0.5°$	0.0236 s
BF, $\delta_\theta = 0.1°$	0.1063 s

TABLE 4. Average time required to compute the optimal position of the MAA using different optimization strategies, for $l = 100$ m, $L_B = 1$ m and $K = 10$.

Optimization strategy	Average computational time
PSO	0.0761 s
BF, $\delta_{x,y} = 5$ cm	0.0270 s
BF, $\delta_{x,y} = 1$ cm	0.5756 s

TABLE 5. Average time required to compute the optimal position and rotation of the MRAA using different optimization strategies, for $\delta_\theta = 1^\circ$, $l = 100$ m, $L_B = 1$ m and $K = 10$.

Optimization strategy	Average computational time
PSO	0.3178 s
BF, $\delta_{x,y} = 10$ cm	1.4346 s
BF, $\delta_{x,y} = 5$ cm	5.5332 s

proves to be highly advantageous in optimization problems with multiple variables, except when the quantization levels are significantly low. It is important to note that adopting large discrete steps for the array's linear movement may significantly degrade the system's overall performance in terms of mean per-user achievable SE, as the MAA or MRAA may end up in a sub-optimal position.

D. SPEED OF SERVO MOTORS AND TIMING REQUIREMENTS

After computing the optimal position and/or rotation of the antenna array, the system needs to physically move and/or rotate the array. The rotation of the array is performed by a servo motor connected to the array, as shown in Fig. 3(a). Commercial high-speed industrial servo motors can change their angular positions within a few milliseconds with very high precision [63], [64]. Thus, the angular position of the array can be changed within a single or a few time slots. On the other hand, the movement of the array within a horizontal plane is performed using linear motion systems, with consist on servo motors and slide tracks, as illustrated in Fig. 3(b). Commercial high speed and high precision linear motion systems have maximum speed on the order of a few meters/second [65], [66]. Thus, the two-dimensional movement of the array is much slower than its rotation. As a consequence, the length of the size of the movement area (i.e., L_B) should not be larger than a few meters in practice to avoid long delays in the communication. Taking into account the speed of the commercial rotation and movement mechanisms, the duration of Phase 3 of the protocol illustrated in Fig. 4 is on the order of a few seconds,

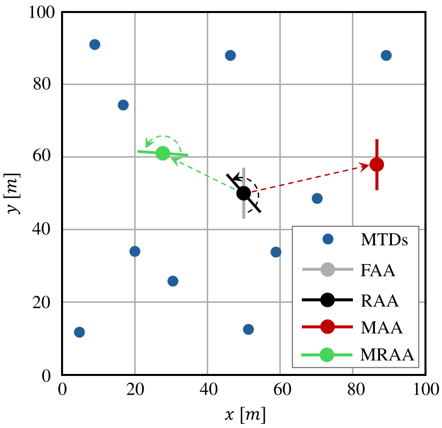

FIGURE 9. Illustration of the simulation setup and the four types of APs considered in this work for $L_A = 100$ m and $K = 10$.

thus longer than the channel coherence time (which is on the order of a few milliseconds) and the phases 1, 2 and 4 (which span single or few time slots.)

IV. NUMERICAL RESULTS

In this section, we present Monte Carlo simulation results to compare the performance achieved by the four different types of APs studied in this work.

A. SIMULATION PARAMETERS

The power attenuation due to the distance (in dB) is modelled using the log-distance path loss model as

$$\beta_k = -L_0 - 10\eta \log_{10}\left(\frac{d_k}{d_0}\right), \tag{34}$$

where d_0 is the reference distance in meters, L_0 is the attenuation owing to the distance at the reference distance (in dB), η is the path loss exponent and d_k is the distance between the k-th MTD and the AP in meters. The attenuation at the reference distance is calculated using the Friis free-space path loss model and given by

$$L_0 = 20\log_{10}\left(\frac{4\pi d_0}{\lambda}\right), \tag{35}$$

where $\lambda = c/f_c$ is the wavelength in meters, c is the speed of light and f_c is the carrier frequency.

The simulation setup is illustrated in Fig. 9. Unless specified otherwise, the simulation parameter values used in this work are provided in Table 6. Considering the selected values of M and h_{AP}, the communication links between any antenna array and any MTD experience far-field propagation conditions (please refer to Appendix A). Additionally, the adopted parameters for the PSO algorithm are listed in Table 7.

The noise power (in Watts) is given by $\sigma_n^2 = N_0 B N_F$, where N_0 is the power spectral density of the thermal noise in W/Hz, B is the signal bandwidth in Hz, and N_F is the noise figure at the receivers. For the computation of the correlation matrices $\mathbf{R}_k$, $\forall k$, we consider $N = 6$ scattering clusters, $\psi_{k,n} \sim \mathcal{U}[\phi_k - 40\circ, \phi_k + 40\circ]$, and $\sigma_\psi = 5\circ$ [33].

TABLE 6. Simulation parameters [31], [33], [67].

Parameter	Symbol	Value
Total number of antenna elements	M	16
Number of active MTDs	K	10
Length of the side of the square area	L_A	100 m
Uplink transmission power	p	100 mW
PSD of the noise	N_0	4×10^{-21} W/Hz
Signal bandwidth	B	20 MHz
Noise figure	N_F	9 dB
Length of the pilot sequences	τ_p	10 samples
Length of the time slot	τ_p	200 samples
Height of the APs	h_{AP}	12 m
Height of the UEs	h_{UE}	1.5 m
Carrier frequency	f_c	3.5 GHz
Normalized inter-antenna spacing	Δ	0.5
Path loss exponent	η	2
Reference distance	d_0	1 m

TABLE 7. Values of the parameters of the PSO Algorithm used for the simulations [61].

Symbol	Parameter	Value
w	Inertial weight	$[0.1, 1.1]$
c_1	Cognitive constant	1.49
c_2	Social constant	1.49
N_{vars}	Number of variables	$[1, 2, 3]$
$\lvert\mathcal{A}\rvert$	Swarm size	$\min\{100, 10N_{\text{vars}}\}$
$N_{\max}$	Maximum number of iterations	$200N_{\text{vars}}$
N_{stall}	Maximum number of stall iterations	20
ϵ	Function tolerance	10^{-6}

B. SIMULATION RESULTS AND DISCUSSIONS

We generate average performance results for networks of K devices by averaging the per-user mean achievable SE over multiple network realizations. In other words, the numerical results correspond to the expected SE performance gains for networks of K devices in the considered setup. For each network realization, the achievable SE of the K devices is obtained by averaging over several channel realizations, i.e., distinct realizations of the channel matrix $\mathbf{H}$. For each network realization, the locations of the MTDs are fixed and uniformly randomly distributed in the coverage area, i.e., $x_k, y_k \sim \mathcal{U}[0, L_A]$. In the case of MAAs, we evaluate the performance achieved with different sizes of the movement area, i.e., different values of L_B. Note that, in practice, the movement area of the MAAs cannot be very large owing to size and costs constraints. Moreover, moving an array over long distances might take a considerable amount of time (which can be longer than the coherence time of the wireless channel,[9]) even when high-speed servo motors are utilized.

[9]In this work, we consider a static scenario where the MTDs do not move. However, in dynamic environments where MTDs or people/objects are moving faster than the AP movement, the coherence time of the channel would be shorter than the moving speed of the AP.

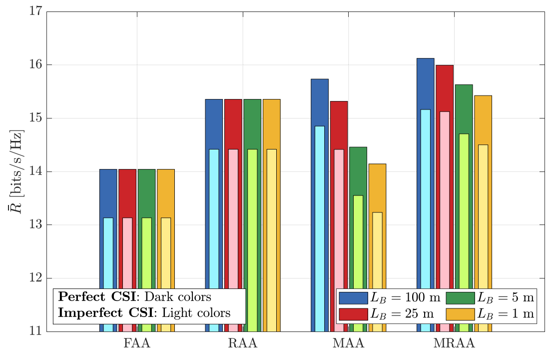

FIGURE 10. Mean per-user achievable SE for all the schemes studied in this work, considering perfect and imperfect CSI, $\kappa = 10$ dB, and $\sigma_e^2 = -10$ dB.

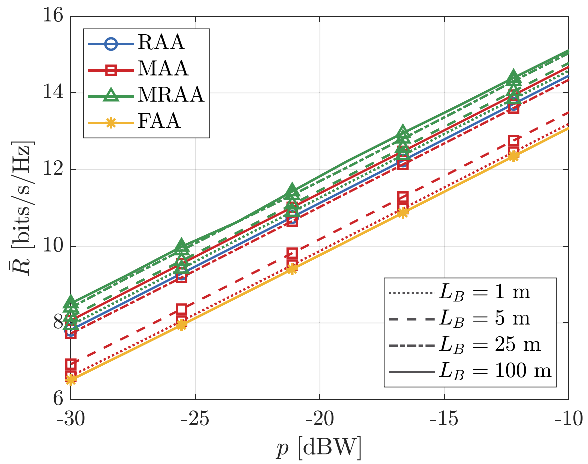

FIGURE 11. Mean per-user achievable SE versus uplink transmit power for $\kappa = 10$ dB and $\sigma_e^2 = -10$ dB.

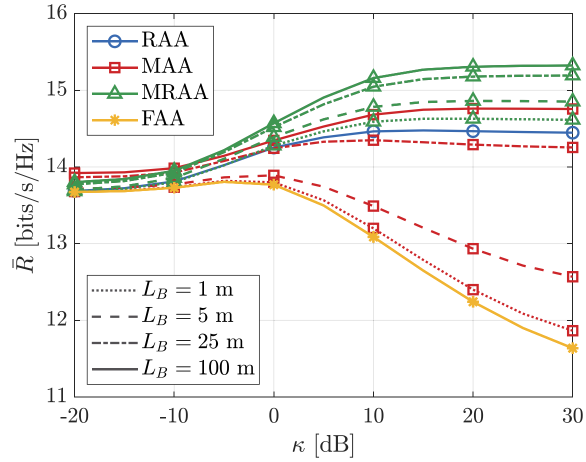

FIGURE 12. Mean per-user achievable SE versus the Rician factor κ, for $\sigma_e^2 = -10$ dB.

Thus, the numerical results for the case of $L_B = L_A = 100$ m, that is, when the movement area covers the whole coverage area, are hypothetical results that represent an ideal scenario and are utilized here solely for benchmark purposes.

We first investigate the impact of the imperfect CSI to the SE. The bar graphs in Fig. 10 show the mean per-user achievable SE for all the schemes studied in this work, considering perfect and imperfect CSI, $\kappa = 10$ dB, and $\sigma_e^2 = -10$ dB. In the case of MAA and MRAA, the figure also shows how the achievable SE decreases as the size of the square movement area reduces. The performance of the FAA and RAA do not vary with L_B since they do not move. As expected, the channel estimation errors reduce $\bar{R}$. Interestingly, the impact is similar to all the antenna schemes and does not vary with the size of the square movement area. From now on, we consider only the case of imperfect CSI.

The curves in Fig. 11 depict that the performance gains obtained with the optimal movement and/or rotation of the antenna array are observed over a wide range of SNRs. More specifically, this figure shows the mean per-user achievable SE in the uplink versus the fixed transmit power p of the active MTDs for all the schemes considered in this work and for $\kappa = 10$ dB, $\sigma_e^2 = -10$ dB, and different sizes of the square movement area. As expected, the achievable SE values increase substantially with p for all the considered setups. Nevertheless, we note that the performance improvement of the RAA, MAA, and MRAA over the FAA is constant over the wide range of values of p. Thus, we set $p = 0.1$ W from now on [68], [69], [70].

Fig. 12 shows the mean per-user achievable SE versus the Rician factor. In the case of an AP equipped with an FAA or a MAA with a very constrained movement area, we observe that the achievable SE decreases with the Rician factor, while it increases with κ when we adopt a RAA or a MAA with a large movement area. As shown in [71], the correlation among the channel vectors increases with κ, which affects the performance obtained with ZF in the case of an FAA or MAA with a small movement area. Nevertheless, by rotating and/or moving the antenna array over a larger area, the AP can find an optimal position and/or rotation that reduces the correlation among the channel vectors. Note that the performance gains obtained with the optimal rotations or movements become very significant when the LoS component is very strong. As expected, the best performance is achieved with the MRAA, since it has three degrees of freedom for the movements. However, it features the most complex and expensive setup. The MAA, which has two degrees of freedom for the movement, outperforms the RAA only when the movement area covers the whole coverage area. It is very interesting to observe that the RAA outperforms the MAA in the case of $L_B = 25$ m, which corresponds to a very large movement area.

Fig. 13 shows the mean per-user achievable SE versus the dimensions of the movement area for $\kappa = 10$ dB, i.e., a situation where the LoS component of the channel vectors is very strong. When $L_B \to 0$ m, the performance obtained with the MAA converges to the performance obtained with the FAA, while the performance obtained with the MRAA converges to the performance obtained with the RAA, as expected. As we increase the size of the movement area,

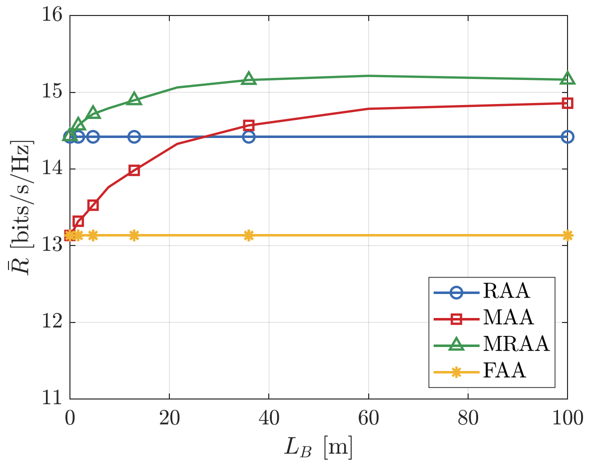

FIGURE 13. Mean per-user achievable SE versus dimensions of the movement area, for $\kappa = 10$ dB and $\sigma_e^2 = -10$ dB.

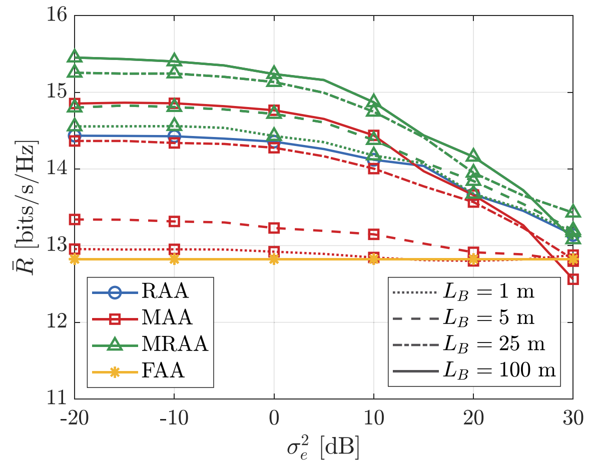

FIGURE 14. Mean per-user achievable SE versus variance of the localization error considering $\kappa = 10$ dB.

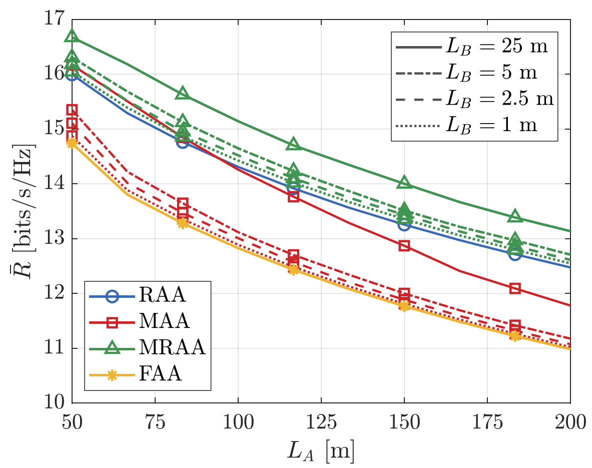

FIGURE 15. Mean per-user achievable SE versus dimensions of the coverage area, for $\kappa = 10$ dB and $\sigma_e^2 = -10$ dB.

the performance gains obtained with the movement of the antenna array becomes noticeable. We observe again that the MRAA always presents the best performance. When adopting the MAA, we need a considerably large movement area ($L_B > 25$ m) in order to achieve the same performance that can be obtained by simply rotating the antenna array. Note also that the performance improvement obtained by increasing the size of the movement area is negligible for $L_B \geq 50$ m.

Fig. 14 shows the mean per-user achievable SE versus the variance of the localization error. We observe that all the optimal rotations and movements of the antenna arrays bring noticeable performance improvements even when the accuracy of the localization information is poor. However, the performance gains on the achievable SE when compared to the case of an FAA decay rapidly for $\sigma_e^2 \geq 10$ dB. We again observe that the best performance is achieved by the MRAA, followed by the MAA and then the RAA. Nevertheless, note that increasing the accuracy of the localization information to sub-cm or mm levels do not yield performance improvements.

Finally, Fig. 15 shows the mean per-user achievable SE versus the dimensions of the coverage area, for $M = 16$ and $K = 10$. As expected, the achievable SE decreases with L_A for any of the considered setups due to the increased path-losses. We also observe that rotating and/or moving the antenna array always improves the mean per-user achievable SE compared to the case of an FAA. Nonetheless, when the movement area is very constrained, specifically $L_B = 1$ m, the performance improvement obtained by moving the array on the horizontal plane is very small. Therefore, a larger movement area is essential to achieve substantial improvements in spectral efficiency. It is noteworthy that the RAA always outperforms the MAAs with $L_B = \{1, 2.5, 5\}$ m, and it can even outperform the MAA with $L_B = 25$ m when $L_A > 95$ m, which corresponds to a setup with a large movement area. This finding demonstrates that rotating the array provides greater improvements in the mean per-user achievable SE compared to moving the array along the horizontal plane, even when the movement area on the horizontal plane is relatively large. Finally, note that the best performance is always achieved by the MRAA, which has more degrees of freedom at the cost of the most complex setup.

Overall, the numerical results show that when the active devices experience strong LoS conditions (that is, when the Rician factor is high), the antenna arrays with movement and/or rotation capabilities offer better performance (in terms of the mean per-user achievable SE in the uplink) compared to the case of an antenna array without any movement capability. This occurs because, under strong LoS conditions, the system's performance is highly dependent on the array geometry and its relative position to the active MTDs. When the 2D movement area is not constrained, that is, when the MAA and the MRAA can be positioned in any point of the coverage area, the best performance is achieved by the MRAA (which has three degrees of freedom for movement and utilizes three servo motors), followed by the MAA (two degrees of freedom, two servo motors) and then by the RAA (one degree of freedom, one servo motor). Nevertheless, the movements

TABLE 8. Mean and variance of the execution time required for PSO to finish, considering $\kappa = 10$ dB and $\sigma_e^2 = -10$ dB.

Setup	L_B	Mean	Variance
RAA	N/A	0.0912 s	0.0011 s^2
MAA	1 m	0.1109 s	0.0013 s^2
	5 m	0.1371 s	0.0041 s^2
	25 m	0.2062 s	0.0075 s^2
	100 m	0.5253 s	0.1950 s^2
MRAA	1 m	0.3362 s	0.0108 s^2
	5 m	0.3732 s	0.0163 s^2
	25 m	0.4528 s	0.0366 s^2
	100 m	0.6359 s	0.0817 s^2

of the arrays on the horizontal plane directions need to be constrained in practice due to size, costs, complexity and latency limitations. Moving the array along large distances might induce very high latency because servo motors do not have infinite speed in the real world. In order words, it is not feasible to utilize large values of L_B in practice. For any value of L_B, the MRAA always presents the best performance, since it has more DoFs for movement, but at the cost of the most complex setup. When the 2D movement area of the MAA is constrained (i.e., when L_B is kept small), the RAA outperforms it, while simultaneously presenting a significantly lower size, complexity, and deployment and maintenance costs. Thus, we conclude that the rotational capability of the antenna array is the DoF that strikes the best balance between performance gains and cost/complexity.

C. COMPLEXITY ANALYSIS OF PSO

The simulations ran on a personal computer having Windows 11, Intel Core i5-1340P processor and 32 GB of RAM memory. Besides, we utilized MATLAB version R2024b. The PSO was implemented on MATLAB using the `particleswarm` built-in function [61]. Since we utilized a built-in function of MATLAB, it is very difficult to measure the complexity of the PSO in terms of metrics such as number of float-point operations (FLOPs). Thus, we decided to analyse the computational complexity of our PSO solution in terms of the mean and the variance of the required time for the optimization algorithm to finish. This time can be measured in MATLAB using the functions `tic;toc` or `cputime`.

The mean and variance of the execution time necessary to compute the optimal position and/or rotation of the antenna array can be found in Table 8. In the case of MAA and MRAA, we consider different values for the dimension of the movement area. The PSO converges when the relative change in the value of the objective function over a given number of "maximum stall iterations" is less than the "function tolerance" [61]. As expected, the required execution time increases with the number of DoFs for movement (i.e., the number of optimization variables). The optimization task executed for the RAA is the fastest one, followed by the optimization required for the MAA and then by the MRAA. We also observe that the required execution time slightly increases with the dimension of the movement area, since the particles of the PSO algorithm need to find the global optimum over a larger search area. The results in Table 8 evince another advantage of the RAA over the MAA: in addition to presenting superior performance when the movement area is constrained, the computation of the optimal angular position is faster than the computation of the optimal position on the horizontal plane.

Note that the required time to compute the optimal movement and/or rotation of the antenna array using PSO in practical hardware would be multiple orders of magnitude smaller than the times listed in Table 8. However, the physical movement and/or rotation of the array requires an amount of time that is significantly larger than the coherence time of the wireless channel (which is in the order of a few milliseconds,[10]) thus it would be unfeasible to move and/or rotate the array in each time slot. For this reason, these tasks must be executed before the data transmission phase such that the position and/or rotation of the antenna array is kept unchanged over multiple time slots. Moreover, while phases 1, 2 and 4 of the protocol proposed in Section II-B can fit within a single or few time slots, phase 3 needs to last at least a couple of seconds to accommodate the computation of the optimal position and/or rotation of the array and also the physical movement/rotation.

V. CONCLUSION

In this work, we compared the performance of MAAs, which are able to move on the horizontal plane using two servo motors, cables and slide tracks, with RAAs, which are equipped a single servo motor and that can rotate on its own axis. We also proposed the combination of both schemes into MRAAs, which are arrays that can move on the horizontal plane and also rotate. The optimal position and/or rotation of the arrays is computed based on estimates of the locations of the active MTDs and using PSO. Our numerical results show that the MAAs outperform the RAAs when their movement area is large enough, but at the cost of a bulkier setup with higher maintenance and deployment costs. When the movement area of the arrays is constrained, the RAAs perform better and also correspond to a simpler and cheaper system. All the proposed techniques offer significant performance gains in terms of mean per-user achievable SE when compared to FAAs when the LoS component of the channel vectors is strong, and all the schemes are robust against imperfect location estimates.

APPENDIX A
FAR-FIELD PROPAGATION CONDITIONS

The Fraunhofer distance determines the threshold between the near-field and far-field propagation, and is given by $d_F =$

[10]The coherence time of the channel can be approximated as the time it takes to move one quarter of the wavelength λ, that is, $T_c = \lambda/4v$, where v is the velocity of the MTD [35]. Considering $f_c = 3.5$ GHz and a walking speed of 1.4 m/s, the coherence time is approximately $T_c = 15$ ms.

$2D^2/\lambda$ [72], where D is the largest dimension of the antenna array, $\lambda = c/f_c$ is the wavelength, c is the speed of the light and f_c is the carrier frequency. In the case of an ULA with M antenna elements spaced by half-wavelength, the length of the ULA is $D_{\text{ULA}} = (M-1)\lambda/2$.

Considering that a device can be located right bellow an AP in an indoor setting, the minimum height of the AP required to ensure far-field propagation conditions for all the devices is given by

$$\begin{aligned} h_{\text{AP}}^{\min} &= d_F + h_{\text{device}} \\ &= \frac{2}{\lambda}\left((M-1)\frac{\lambda}{2}\right)^2 + h_{\text{device}} \\ &= \frac{\lambda}{2}(M-1)^2 + h_{\text{device}}. \end{aligned} \tag{36}$$

Considering $f_c = 3.5$ GHz, $M = 16$, $h_{\text{device}} = 1.5$ m, we obtain $D_{\text{ULA}} = 0.64$ m and $d_F = 9.64$ m. Thus, the minimum height of the APs is $h_{\text{AP}}^{\min} = 11.14$ m.

REFERENCES

[1] C. Lim, T. Yoo, B. Clerckx, B. Lee, and B. Shim, "Recent trend of multiuser MIMO in LTE-advanced," *IEEE Commun. Mag.*, vol. 51, no. 3, pp. 127–135, Mar. 2013.

[2] F. Boccardi, R. W. Heath, A. Lozano, T. L. Marzetta, and P. Popovski, "Five disruptive technology directions for 5G," *IEEE Commun. Mag.*, vol. 52, no. 2, pp. 74–80, Feb. 2014.

[3] S. Avallone, P. Imputato, G. Redieteab, C. Ghosh, and S. Roy, "Will OFDMA improve the performance of 802.11 WiFi networks?" *IEEE Wireless Commun.*, vol. 28, no. 3, pp. 100–107, Jun. 2021.

[4] R. W. Heath Jr and A. Lozano, *Foundations of MIMO Communication*. Cambridge, U.K.: Cambridge Univ. Press, 2018.

[5] E. N. Tominaga, O. L. A. López, T. Svensson, R. D. Souza, and H. Alves, "On the spectral efficiency of indoor wireless networks with a rotary uniform linear array," 2024, *arXiv:2402.05583*.

[6] J. Li, Z. Lin, S. G. Razul, A. A. Kumar, Y. Zheng, and C.-M. See, "DOA estimation with a rotational uniform linear array (RULA) and unknown spatial noise covariance," *Multidimens. Syst. Signal Process.*, vol. 29, pp. 537–561, Apr. 2018.

[7] H. Do, N. Lee, and A. Lozano, "Reconfigurable ULAs for line-of-sight MIMO transmission," *IEEE Trans. Wireless Commun.*, vol. 20, no. 5, pp. 2933–2947, May 2021.

[8] O. L. A. López, F. A. Monteiro, H. Alves, R. Zhang, and M. Latva-Aho, "A low-complexity beamforming design for multiuser wireless energy transfer," *IEEE Wireless Commun. Lett.*, vol. 10, no. 1, pp. 58–62, Jan. 2021.

[9] O. L. A. López, H. Alves, S. Montejo-Sánchez, R. D. Souza, and M. Latva-aho, "CSI-free rotary antenna beamforming for massive RF wireless energy transfer," *IEEE Internet Things J.*, vol. 9, no. 10, pp. 7375–7387, May 2022.

[10] K. Lin et al., "On CSI-free Multiantenna schemes for massive wireless-powered underground sensor networks," *IEEE Internet Things J.*, vol. 10, no. 19, pp. 17557–17570, Oct. 2023.

[11] A. Zubow, A. Memedi, and F. Dressler, "Towards hybrid electronic-mechanical beamforming for IEEE 802.11ad," in *Proc. 18th Wireless Demand Netw. Syst. Serv. Conf. (WONS)*, 2023, pp. 88–91.

[12] Q. Wu, B. Zheng, T. Ma, and R. Zhang, "Modeling and optimization for rotatable antenna enabled wireless communication," 2024, *arXiv:2411.08411*.

[13] L. Zhu, W. Ma, and R. Zhang, "Movable antennas for wireless communication: Opportunities and challenges," *IEEE Commun. Mag.*, vol. 62, no. 6, pp. 114–120, Jun. 2024.

[14] Z. Xiao et al., "Multiuser communications with movable-antenna base station: Joint antenna positioning, receive combining, and power control," *IEEE Trans. Wireless Commun.*, vol. 23, no. 12, pp. 19744–19759, Dec. 2024.

[15] L. Zhu, W. Ma, and R. Zhang, "Movable-antenna array enhanced beamforming: Achieving full array gain with null steering," *IEEE Commun. Lett.*, vol. 27, no. 12, pp. 3340–3344, Dec. 2023.

[16] J.-M. Kang, "Deep learning enabled multicast beamforming with movable antenna array," *IEEE Wireless Commun. Lett.*, vol. 13, no. 7, pp. 1848–1852, Jul. 2024.

[17] W. Mei, X. Wei, B. Ning, Z. Chen, and R. Zhang, "Movable-antenna position optimization: A graph-based approach," *IEEE Wireless Commun. Lett.*, vol. 13, no. 7, pp. 1853–1857, Jul. 2024.

[18] L. Zhu, W. Ma, and R. Zhang, "Modeling and performance analysis for movable antenna enabled wireless communications," *IEEE Trans. Wireless Commun.*, vol. 23, no. 6, pp. 6234–6250, Jun. 2024.

[19] L. Zhu, W. Ma, B. Ning, and R. Zhang, "Movable-antenna enhanced multiuser communication via antenna position optimization," *IEEE Trans. Wireless Commun.*, vol. 23, no. 7, pp. 7214–7229, Jun. 2024.

[20] Y. Wu, D. Xu, D. W. K. Ng, W. Gerstacker, and R. Schober, "Movable antenna-enhanced multiuser communication: Jointly optimal discrete antenna positioning and beamforming," in *Proc. IEEE Global Commun. Conf. (GLOBECOM)*, 2023, pp. 7508–7513.

[21] B. Feng, Y. Wu, X.-G. Xia, and C. Xiao, "Weighted sum-rate maximization for movable antenna-enhanced wireless networks," *IEEE Wireless Commun. Lett.*, vol. 13, no. 6, pp. 1770–1774, Jun. 2024.

[22] X. Wei, W. Mei, D. Wang, B. Ning, and Z. Chen, "Joint beamforming and antenna position optimization for movable antenna-assisted spectrum sharing," *IEEE Wireless Commun. Lett.*, vol. 13, no. 9, pp. 2502–2506, Sep. 2024.

[23] B. Ning et al., "Movable antenna-enhanced wireless communications: General architectures and implementation methods," 2024, *arXiv:2407.15448*.

[24] E. N. Tominaga, O. L. A. López, T. Svensson, R. D. Souza, and H. Alves, "Distributed MIMO networks with rotary ULAs for indoor scenarios under Rician fading," *IEEE Open J. Commun. Soc.*, vol. 5, pp. 6367–6380, 2024.

[25] X. Shao, R. Zhang, and R. Schober, "Exploiting six-dimensional movable antenna for wireless sensing," *IEEE Wireless Commun. Lett.*, vol. 14, no. 2, pp. 265–269, Feb. 2025.

[26] X. Shao, Q. Jiang, and R. Zhang, "6D movable antenna based on user distribution: Modeling and optimization," 2024, *arXiv:2403.08123*.

[27] L. Zhu et al., "A tutorial on movable antennas for wireless networks," *IEEE Commun. Surveys Tuts.*, early access, Feb. 27, 2025, doi: 10.1109/COMST.2025.3546373.

[28] H. Wang, H. Zhao, W. Wu, J. Xiong, D. Ma, and J. Wei, "Deployment algorithms of flying base stations: 5G and beyond with UAVs," *IEEE Internet Things J.*, vol. 6, no. 6, pp. 10009–10027, Dec. 2019.

[29] G. Amponis et al., "Drones in B5G/6G networks as flying base stations," *Drones*, vol. 6, no. 2, p. 39, 2022.

[30] S. A. H. Mohsan, N. Q. H. Othman, Y. Li, M. H. Alsharif, and M. A. Khan, "Unmanned aerial vehicles (UAVs): Practical aspects, applications, open challenges, security issues, and future trends," *Intell. Services Robot.*, vol. 16, no. 1, pp. 109–137, 2023.

[31] H. Q. Ngo, A. Ashikhmin, H. Yang, E. G. Larsson, and T. L. Marzetta, "Cell-free massive MIMO versus small cells," *IEEE Trans. Wireless Commun.*, vol. 16, no. 3, pp. 1834–1850, Mar. 2017.

[32] Z. Chen and E. Björnson, "Channel hardening and Favorable propagation in cell-free massive MIMO with stochastic geometry," *IEEE Trans. Commun.*, vol. 66, no. 11, pp. 5205–5219, Nov. 2018.

[33] O. Özdogan, E. Björnson, and E. G. Larsson, "Massive MIMO with spatially correlated Rician fading channels," *IEEE Trans. Commun.*, vol. 67, no. 5, pp. 3234–3250, May 2019.

[34] D. Kumar, O. L. A. López, A. Tölli, and S. Joshi, "Latency-aware joint transmit beamforming and receive power splitting for SWIPT systems," in *Proc. IEEE 32nd Annu. Int. Symp. Pers. Indoor Mobile Radio Commun. (PIMRC)*, 2021, pp. 490–494.

[35] E. Björnson, J. Hoydis, and L. Sanguinetti, "Massive MIMO networks: Spectral, energy, and hardware efficiency," *Found. Trends® Signal Process.*, vol. 11, nos. 3–4, pp. 154–655, 2017.

[36] C. Wang, T. C.-K. Liu, and X. Dong, "Impact of channel estimation error on the performance of amplify-and-forward two-way relaying," *IEEE Trans. Veh. Technol.*, vol. 61, no. 3, pp. 1197–1207, Mar. 2012.

[37] E. Eraslan, B. Daneshrad, and C.-Y. Lou, "Performance indicator for MIMO MMSE receivers in the presence of channel estimation error," *IEEE Wireless Commun. Lett.*, vol. 2, no. 2, pp. 211–214, Apr. 2013.

[38] O. L. A. López, D. Kumar, R. D. Souza, P. Popovski, A. Tölli, and M. Latva-Aho, "Massive MIMO with radio stripes for indoor wireless energy transfer," *IEEE Trans. Wireless Commun.*, vol. 21, no. 9, pp. 7088–7104, Sep. 2022.

[39] J. Kang and W. Yu, "Scheduling versus contention for massive random access in massive MIMO systems," *IEEE Trans. Commun.*, vol. 70, no. 9, pp. 5811–5824, Sep. 2022.
[40] D. Tse and P. Viswanath, *Fundamentals of Wireless Communication*. Cambridge, U.K.: Cambridge Univ. Press, 2005.
[41] P. Liu, K. Luo, D. Chen, and T. Jiang, "Spectral efficiency analysis of cell-free massive MIMO systems with zero-forcing detector," *IEEE Trans. Wireless Commun.*, vol. 19, no. 2, pp. 795–807, Feb. 2020.
[42] F. Gustafsson and F. Gunnarsson, "Mobile positioning using wireless networks: Possibilities and fundamental limitations based on available wireless network measurements," *IEEE Signal Process. Mag.*, vol. 22, no. 4, pp. 41–53, Jul. 2005.
[43] B. Zhu, Z. Zhang, and J. Cheng, "Outage analysis and beamwidth optimization for positioning-assisted beamforming," *IEEE Commun. Lett.*, vol. 26, no. 7, pp. 1543–1547, Jul. 2022.
[44] "Service requirements for the 5G system," 3GPP, Sophia Antipolis, France, Rep. TS 22.261, 2019.
[45] "Study on NR positioning support; (Release 16)," 3GPP, Sophia Antipolis, France, Rep. TR 38.855, Mar. 2019.
[46] "Study on NR positioning support; (Release 17)," 3GPP, Sophia Antipolis, France, Rep. TR 38.857, Mar. 2021.
[47] H. Wymeersch and G. Seco-Granados, "Radio Localization and sensing—Part-II: State-of-the-art and challenges," *IEEE Commun. Lett.*, vol. 26, no. 12, pp. 2821–2825, Dec. 2022.
[48] J. Nikonowicz, A. Mahmood, M. I. Ashraf, E. Björnson, and M. Gidlund, "Indoor positioning in 5G-advanced: Challenges and solution toward Centimeter-level accuracy with carrier phase enhancements," *IEEE Wireless Commun.*, vol. 31, no. 4, pp. 268–275, Aug. 2024.
[49] R. Maiberger, D. Ezri, and M. Erlihson, "Location based beamforming," in *Proc. IEEE 26th Conv. Elect. Electron. Eng. Israel*, 2010, pp. 000184–000187.
[50] P. Kela et al., "Location based beamforming in 5G ultra-dense networks," in *Proc. IEEE 84th Veh. Technol. Conf. (VTC)*, 2016, pp. 1–7.
[51] S. Yan and R. Malaney, "Location-based beamforming for enhancing secrecy in Rician wiretap channels," *IEEE Trans. Wireless Commun.*, vol. 15, no. 4, pp. 2780–2791, Apr. 2016.
[52] C. Liu and R. Malaney, "Location-based beamforming and physical layer security in Rician wiretap channels," *IEEE Trans. Wireless Commun.*, vol. 15, no. 11, pp. 7847–7857, Nov. 2016.
[53] S. P. Boyd and L. Vandenberghe, *Convex Optimization*. Cambridge, U.K.: Cambridge Univ. Press, 2004.
[54] A. P. Engelbrecht, *Computational Intelligence: An Introduction*. Hoboken, NJ, USA: Wiley, 2007.
[55] J. Kennedy and R. Eberhart, "Particle swarm optimization," in *Proc. Int. Conf. Neural Netw. (ICNN)*, 1995, pp. 1942–1948.
[56] R. V. Kulkarni and G. K. Venayagamoorthy, "Particle swarm optimization in wireless-sensor networks: A brief survey," *IEEE Trans. Syst. Man Cybern. Part-C (Appl. Rev.)*, vol. 41, no. 2, pp. 262–267, Mar. 2011.
[57] N. Jin and Y. Rahmat-Samii, "Advances in particle swarm optimization for antenna designs: Real-number, binary, single-objective and multiobjective implementations," *IEEE Trans. Antennas Propag.*, vol. 55, no. 3, pp. 556–567, Mar. 2007.
[58] F. Shu, W. Gang, and L. Shao-Qian, "Optimal multiuser MIMO linear precoding with LMMSE receiver," *EURASIP J. Wireless Commun. Netw.*, vol. 2009, Aug. 2009, Art. no. 197682, doi: 10.1155/2009/197682.
[59] Y. Hei, X. H. Li, K. C. Yi, and H. Yang, "Novel scheduling strategy for downlink multiuser MIMO system: Particle swarm optimization," *Sci. China Ser. F, Inf. Sci.*, vol. 52, no. 12, pp. 2279–2289, 2009.
[60] C. Knievel, P. A. Hoeher, A. Tyrrell, and G. Auer, "Particle swarm enhanced graph-based channel estimation for MIMO-OFDM," in *Proc. IEEE 73rd Veh. Technol. Conf. (VTC-)*, 2011, pp. 1–5.
[61] (MathWorks, Natick, MA, USA). *Particle Swarm Optimization*. 2024. Accessed: Jun. 20, 2024. [Online]. Available: https://se.mathworks.com/help/gads/particleswarm.html
[62] (MathWorks, Natick, MA, USA). *Particle Swarm Optimization Algorithm*. 2024. Accessed: Jan. 9, 2025. [Online]. Available: https://www.mathworks.com/help/gads/particle-swarm-optimization-algorithm.html
[63] (Constar, Inc., Philadelphia, PA, USA). *Precision Servo Motor*. 2023. [Online]. Available: http://constarmotor.com/productlist/2168.html#E_2189
[64] Yaskawa. "Sigma-5 servo products." 2023. [Online]. Available: https://www.yaskawa.com/products/motion/sigma-5-servo-products
[65] (CSK Motion Technol. Co., Qingdao, China). *Linear Motion Platform*. 2025. [Online]. Available: https://en.cskmotion.com/
[66] Thomson. "Linear motion systems." 2025. [Online]. Available: https://www.thomsonlinear.com/en/index
[67] "Scenarios, frequencies and new field measurements results from two operational factory halls at 3.5 GHz for various antenna configurations," Nokia, Espoo, Finland, Nokia Shanghai Bell Co., Shanghai, China, 3GPP, Sophia Antipolis, France, document TSG RAN WG1 Meeting #95, 3GPP R1-1813177, Nov. 2018. [Online]. Available: https://www.3gpp.org/ftp/tsg_ran/WG1_RL1/TSGR1_95/Docs/
[68] H. Zhang et al., "User-centric cell-free massive MIMO system for indoor industrial networks," *IEEE Trans. Commun.*, vol. 70, no. 11, pp. 7644–7655, Nov. 2022.
[69] J. Ding, M. Nemati, S. R. Pokhrel, O.-S. Park, J. Cho, and F. Adachi, "Enabling grant-free URLLC: An overview of principle and enhancements by massive MIMO," *IEEE Internet Things J.*, vol. 9, no. 1, pp. 384–400, Jan. 2022.
[70] M. U. Khan, E. Testi, M. Chiani, and E. Paolini, "Joint power control and pilot assignment in cell-free massive MIMO using deep learning," *IEEE Open J. Commun. Soc.*, vol. 5, pp. 5260–5275, 2024.
[71] E. N. Tominaga, O. L. A. López, T. Svensson, R. D. Souza, and H. Alves, "On the spectral efficiency of D-MIMO networks under Rician fading," 2024, *arXiv:2410.07159*.
[72] J. Sherman, "Properties of focused apertures in the fresnel region," *IRE Trans. Antennas Propag.*, vol. 10, no. 4, pp. 399–408, 1962.

EDUARDO N. TOMINAGA (Graduate Student Member, IEEE) was born in São Paulo, Brazil, in 1995. He received the B.Sc. degree in electronics engineering from the Federal University of Santa Catarina, Florianópolis, Brazil, in 2019, and the M.Sc. degree in wireless communications engineering from the University of Oulu, Finland, in 2021, where he is currently pursuing the D.Sc. degree in communications engineering with the Centre for Wireless Communications. In 2023, he visited the Nokia Bell Labs, Murray Hill, NJ, USA, and the Communication Systems Group, Chalmers University of Technology, Gothenburg, Sweden. His main research interests include wireless communications and digital signal processing.

ONEL L. A. LÓPEZ (Senior Member, IEEE) was born in Sancti-Spíritus, Cuba, in 1989. He received the B.Sc. (Hons.) degree in electrical engineering from the Central University of Las Villas, Cuba, in 2013, the M.Sc. degree in electrical engineering from the Federal University of Paraná, Brazil, in 2017, and the D.Sc. (Hons.) degree in electrical engineering from the University of Oulu, Finland, in 2020. From 2013 to 2015, he was a Specialist in telematics with Cuban Telecommunications Company (ETECSA). He currently holds an Assistant Professorship (Tenure Track) in sustainable wireless communications engineering with the Centre for Wireless Communications, Oulu, Finland. He is the coauthor of the books titled *Wireless RF Energy Transfer in the Massive IoT Era: Towards Sustainable Zero Energy Networks* (Wiley, 2021) and *Ultra Reliable Low-Latency Communications: Foundations, Enablers, System Design, and Evolution Towards 6G* (Now Publishers, 2023). His research interests include sustainable IoT, energy harvesting, wireless RF energy transfer, wireless connectivity, machine-type communications, and cellular enabled positioning systems. He was a recipient of the 2020 Best Doctoral Thesis Award granted by Academic Engineers and Architects in Finland TEK and Tekniska Föreningen i Finland in 2021 and the 2022 Young Researcher Award in the field of technology in Finland. He was a co-recipient of the 2019 and 2023 IEEE European Conference on Networks and Communications Best Student Paper Award. He is a Collaborator to the 2016 Research Award given by the Cuban Academy of Sciences.

TOMMY SVENSSON (Senior Member, IEEE) received the Ph.D. degree in information theory from Chalmers, Gothenburg, Sweden, in 2003. He is currently a Full Professor of communication systems with the Chalmers University of Technology, Gothenburg, Sweden, where he is also leading the wireless systems research on air interface and wireless backhaul networking technologies for future wireless systems and he was a Coordinator of Communication Engineering Master's Program. He was with Ericsson AB in core networks, radio access networks, and microwave transmission products. He was involved in the European WINNER and ARTIST4G Projects, which made important contributions to the 3GPP LTE Standards, the EU FP7 METIS, and the EU H2020 5GPPP mmMAGIC and 5GCar projects toward 5G, recently the Hexa-X, RISE-6G, and SEMANTIC Projects and the Hexa-X-II, ROBUST-6G and ECO-eNET projects towards 6G. He is also active with WiTECH Antenna Systems Excellence Center, Chalmers targeting cm/mm-wave and (sub)-THz solutions for 6G access, backhaul/fronthaul, and V2X scenarios. He has coauthored six books. His research interests include mobile communication systems, cooperative/context-aided/secure communications, mm-wave/sub-THz communications, C-V2X, JCAS, satellite networks, and sustainability.

RICHARD D. SOUZA (Senior Member, IEEE) received the D.Sc. degree in electrical engineering from the Federal University of Santa Catarina (UFSC), Florianópolis, Brazil, in 2003. From 2004 to 2016, he was with the Federal University of Technology–Paraná, Curitiba, Brazil. Since 2017, he has been with UFSC, where he is a Professor with the Department of Electrical and Electronics Engineering. His research interests are in the areas of wireless communications and signal processing. He is the Supervisor of the Awarded Best Ph.D. Thesis in Electrical Engineering in Brazil in 2014, and a Co-Recipient of the 2016 Research Award from the Cuban Academy of Sciences. He has served as an Editor or an Associate Editor for *Journal of Communications and Information Systems*, IEEE COMMUNICATIONS LETTERS, the IEEE TRANSACTIONS ON VEHICULAR TECHNOLOGY, the IEEE TRANSACTIONS ON COMMUNICATIONS, and IEEE INTERNET OF THINGS JOURNAL.

HIRLEY ALVES (Member, IEEE) received the B.Sc. and M.Sc. degrees in electrical engineering from the Federal University of Technology-Paraná (UTFPR), Curitiba, Brazil, in 2010 and 2011, respectively, and the Dual D.Sc. degree from the University of Oulu, Oulu, Finland, and UTFPR in 2015. He is an Associate Professor and a Head of the Machine-type Wireless Communications Group, 6G Flagship Centre for Wireless Communications, University of Oulu. He is actively working on massive connectivity and ultrareliable low latency communications for future wireless networks, 5G and 6G, full-duplex communications, and physical-layer security. He leads the MTC activities for the 6G Flagship Program. He has received several awards and has been the Organizer, the Chair, the TPC, and the Tutorial Lecturer for several renowned international conferences. He is the General Chair of the ISWCS'2019 and the General Co-Chair of the 1st 6G Wireless Summit, Levi 2019, and ISWCS 2021.